Supporting Information

Tetraphenylethylene embedded [1₅]paracyclophane: AIEgen and macrocycle merged novel supramolecular hosts used for sensing Ni²⁺ ions

Kaiya Wang,[1,†] Xingyi Huang,[1,†] Makesh Mohan,[1,†] Kaituo Zhang,[1] Minzan Zuo,[1] Yuhong Shen,[1] Yue Zhao,[2] Jochen Niemeyer,[3] and Xiao-Yu Hu*,[1]

[1] College of Materials Science and Technology, Nanjing University of Aeronautics and Astronautics, Nanjing 211106, China

[2] School of Chemistry and Chemical Engineering, Nanjing University, Nanjing, 210023, China

[3] Faculty of Chemistry (Organic Chemistry) and Center for Nanointegration Duisburg-Essen (CENIDE), University of Duisburg-Essen, 45117 Essen, Germany

† These authors contributed equally to this work.

Table of Content

1. General information

The commercially available reagents and solvents were either employed as purchased or dried according to procedures described in the literature. [1$_5$]paracyclophane ([1$_5$]**PCP**) was synthesized according to previous reported method.[S1] All reactions were performed under nitrogen atmosphere unless otherwise stated. Analytical thin layer chromatography (TLC) was performed using 0.25 mm silica gel plates. Column chromatography was performed with silica gel (200-300 mesh) produced by Shanghai Titan Scientific Co., Ltd. All yields were given as isolated yields. ^{1}H and ^{13}C NMR spectra were recorded on a Bruker Avance 400 MHz spectrometer with internal standard tetramethylsilane (TMS) and solvent signals as internal references at 298 K, and the chemical shifts (δ) were reported in ppm and coupling constant (J) values were given in Hz. High-resolution electrospray ionization mass spectra (HR-ESI-MS) were recorded on an Agilent 6540Q-TOF LCMS equipped with an electrospray ionization (ESI) probe operating in positive-ion mode with direct infusion. UV-visible spectra were recorded with a Shimadzu UV 1780 UV-Vis Spectrophotometer. Fluorescence spectra were recorded on a Gangdong SCI F-380 Fluorescence spectrophotometer. Transmission electron microscopy (TEM) investigations were carried out using a JEM-2100 instrument. The fluorescence lifetimes were measured employing time correlated single photon counting on a FLS980 instrument (Edinburg Instruments Ltd., Livingstone, UK) with a pulsed xenon lamp. The quantum yields were carried out on a FLS980 instrument with the integrating sphere.

2. Synthesis and characterization of *m*-TPE Mono-[1$_5$]PCP and *m*-TPE Di-[1$_5$]PCP
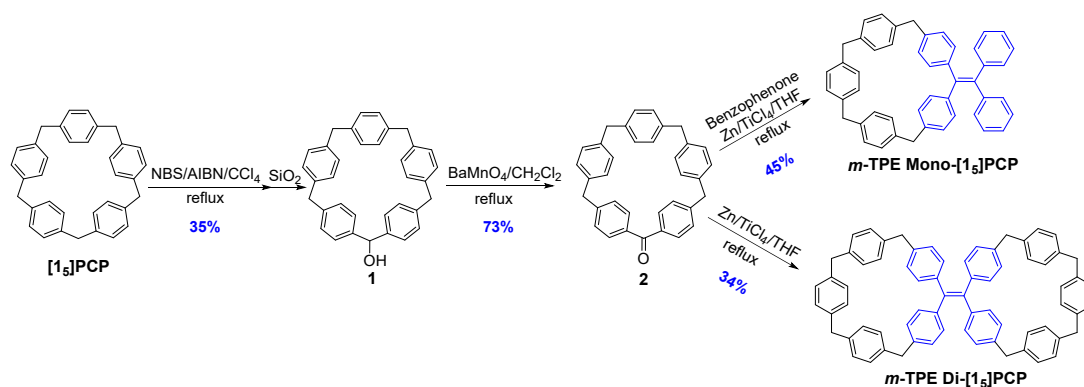
Scheme S1. Synthesis of *m*-TPE Mono[1$_5$]PCP and *m*-TPE Mono[1$_5$]PCP.
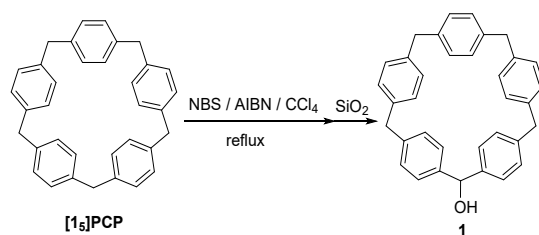
Scheme S2. Synthesis of compound **1**.

The synthesis of mono-functionalized paracyclophane **1** was adapted from a previously reported method.[S2] To a solution of **[1₅]PCP** (869 mg, 1.93 mmol) in CCl_4 (100 mL), N-Bromosuccinimide (NBS, 262.2 mg, 1.473 mmol) and 2,2'-azobis(2-methylpropionitrile) (AIBN, 20 mg, 0.12 mmol) were added under the protection of N_2. The mixture was stirred for 15 mins at room temperature before reflux, and the color of the solution gradually turned into light yellow. After about 2 h, another portion of NBS (150 mg, 0.843 mmol) was added again, and the reaction was carried out overnight. Silica gel was added and the color of the solution changed to dark black. The solution was then concentrated. The crude product was purified by silica gel chromatography using petroleum ether/dichloromethane (1/1~1/2, *v/v*, R_f = 0.3) as the eluent to give compound **1** (315 mg, 0.676 mmol, 35%) as a white solid. ¹H NMR (400 MHz, $CDCl_3$, 298 K) δ 7.15 (d, J = 8.1 Hz, 4H), 7.03 (d, J= 8.1 Hz, 6H), 6.96 (m, 10H), 5.73 (s, 1H), 3.78 (m, 8H); ¹³C NMR (100 MHz, $CDCl_3$, 298 K) δ 140.91, 139.92, 138.46, 138.33, 138.12, 127.60, 127.57, 127.56, 127.52, 124.92, 40.43, 40.33, 28.68. HR-ESI-MS: m/z calcd. [M−H]⁻ 465.2218, found 465.2216.

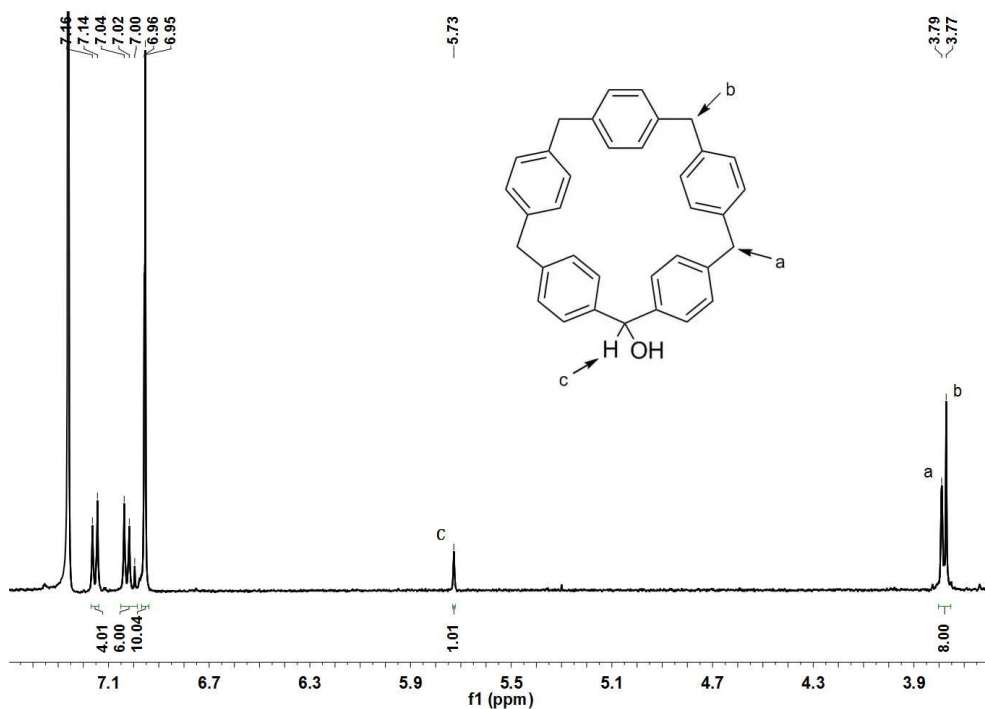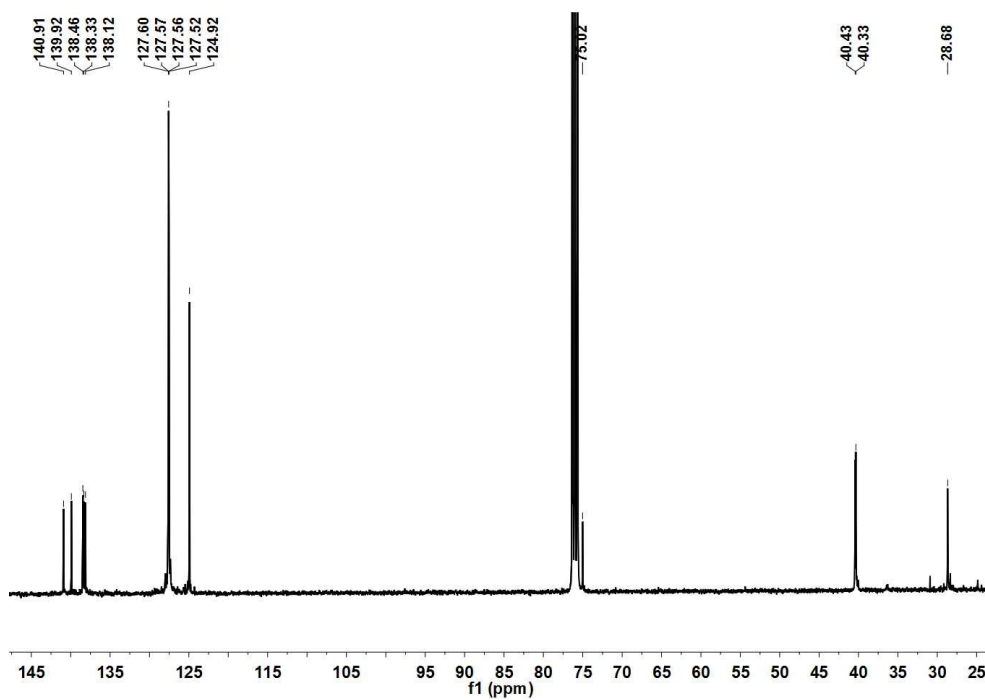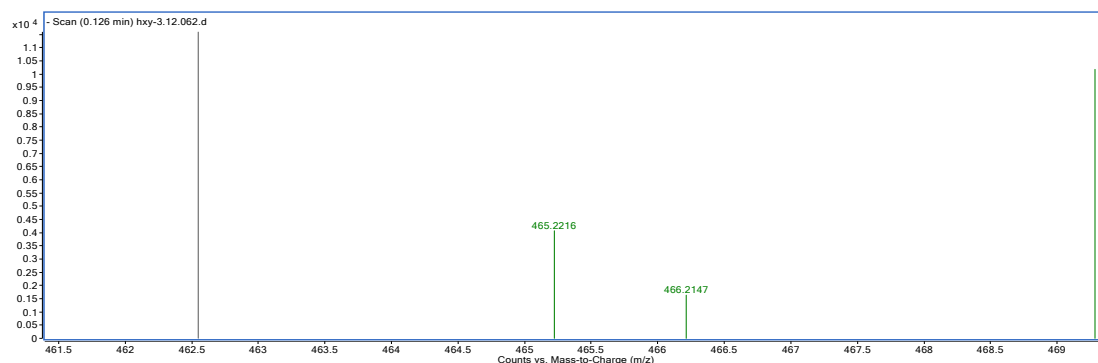**Fig. S1**. ^{1}H NMR spectrum of compound **1** in CDCl$_3$.

Fig. S2. ^{13}C NMR spectrum of compound **1** in CDCl$_3$.

Fig. S3. HR-ESI-MS data for compound **1** (Calculated [M−H]⁻: $C_{35}H_{29}O^-$ = 465.2218, Found: 465.2216).
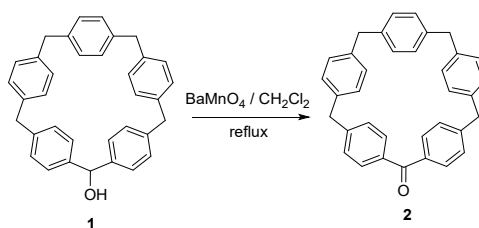
Scheme S3. Synthesis of compound **2**.

Compound **1** (415 mg, 0.891 mmol) and BaMnO₄ (1007.84 mg, 2.68 mmol) were dissolved in dichloromethane (10 mL). The mixture was stirred and heated to reflux for 3 h. The resulting solution was filtered over celite and concentrated. Column chromatography (petroleum ether/dichloromethane = 1/1, *v/v*, R_f = 0.5) gave compound **2** (300 mg, 0.647 mmol, 73%) as a white solid. ¹H NMR (400 MHz, CDCl₃, 298 K) δ 7.24 (d, *J* = 8.3 Hz, 4H), 7.15 (d, *J* = 7.9 Hz, 4H), 7.05 (d, *J* = 8.0 Hz, 4H), 6.93 (s, 4H), 6.90 (d, *J* = 8.2 Hz, 4H), 3.96 (s, 4H), 3.88 (s, 4H); ¹³C NMR (100 MHz, CDCl₃, 298 K) δ 197.99, 146.68, 139.57, 139.31, 138.52, 136.44, 129.51, 129.47, 128.18, 127.90, 41.18, 41.10. HR-ESI-MS: m/z calcd. [M+H]⁺ 465.2218, found 465.2212.

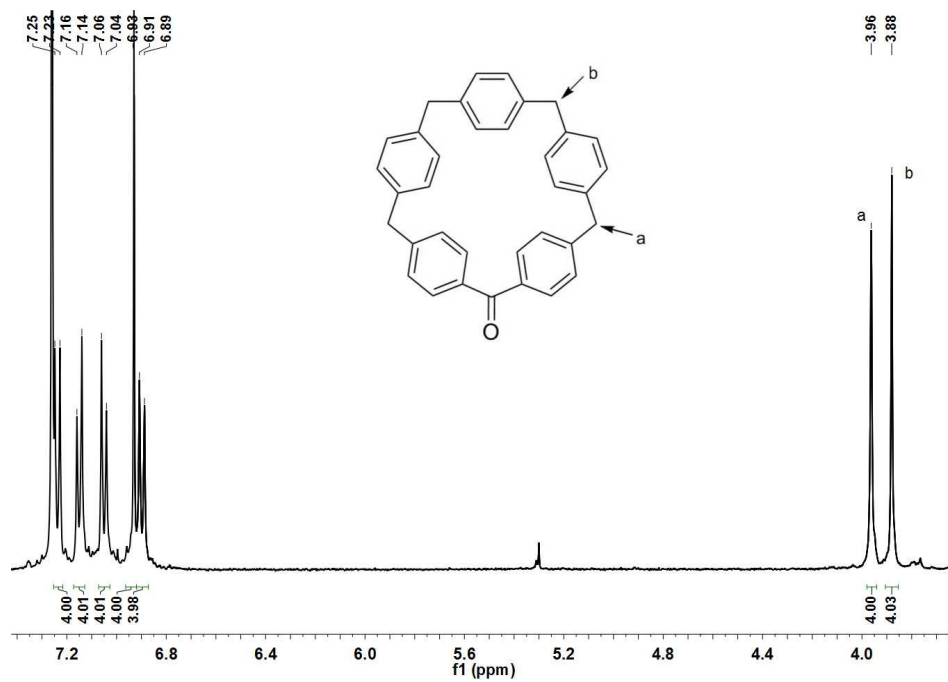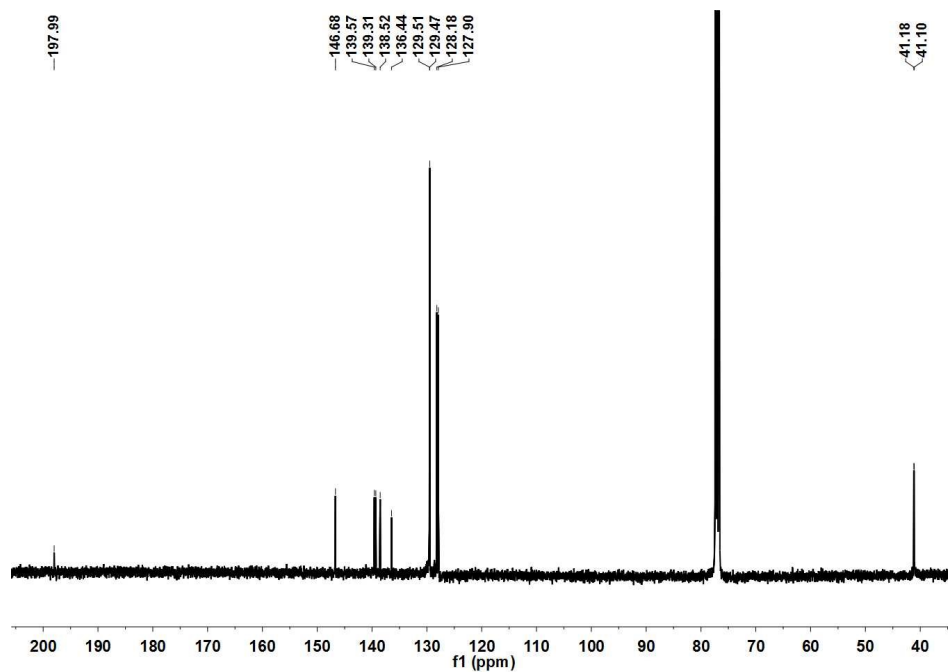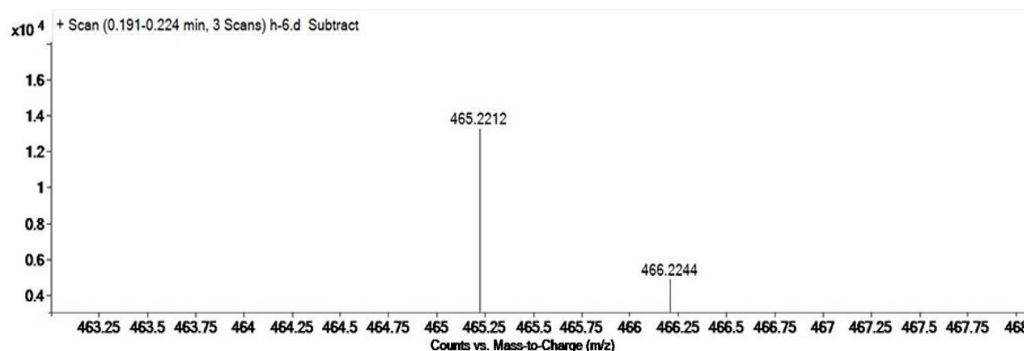**Fig. S4**. ^{1}H NMR spectrum of compound **2** in CDCl$_3$.
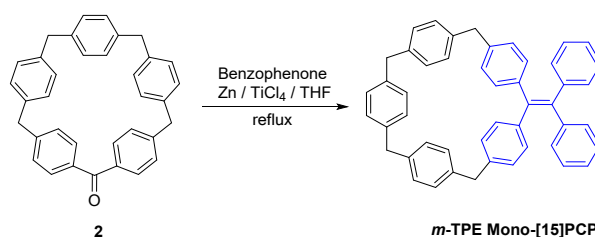

Fig. S5. ^{13}C NMR spectrum of compound **2** in CDCl$_3$.

Fig. S6. HR-ESI-MS data for compound **2** (Calculated [M+H]$^+$: C$_{35}$H$_{29}$O$^+$ = 465.2218, Found: 465.2212).

Scheme S4. Synthesis of compound *m*-TPE Mono-[1$_5$]PCP.

A 50 mL pressure-resistant bottle was charged with zinc powder (565.14 mg, 8.64 mmol), compound **2** (100 mg, 0.216 mmol), benzophenone (393.6 mg, 2.16 mmol), and anhydrous THF (10 mL) under N$_2$ protection. The mixture was cooled to –10 ˚C for 30 mins. Then TiCl$_4$ (0.475 mL, 4.32 mmol) was added and the solution was refluxed overnight. The reaction was quenched by saturated NaHCO$_3$ solution (10 mL). After filtration, the solvent was removed under reduced pressure, the residue was dissolved in CH$_2$Cl$_2$ (200 mL), and washed with 1 M HCl (2 × 100 mL) and brine (2 × 100 mL). The organic phase was dried over anhydrous Na$_2$SO$_4$ and the solvent was removed under vacuum. **m-TPE Mono-[1$_5$]PCP** (60 mg, 0.0976 mmol, 45%) was obtained by column chromatography (PE/dichloromethane = 8/1~2/1, *v/v*, R$_f$ = 0.55). ^{1}H NMR (400 MHz, CDCl$_3$, 298 K) δ 7.10 (d, *J* = 7.1 Hz, 7H), 7.06 – 7.01 (m, 8H), 6.97 (m, 8H), 6.70 (s, 7H), 3.80 (s, 4H), 3.74 (s, 4H); ^{13}C NMR (100 MHz, CDCl$_3$, 298 K) δ 142.64, 140.53, 139.74, 138.60, 138.53, 138.36, 138.28, 138.12, 130.21, 129.90, 128.12, 127.60, 127.38, 126.71, 126.59, 125.23, 40.41, 40.14. HR-ESI-MS: m/z calcd. [M+Na]$^+$ 637.2871, found 637.2859.
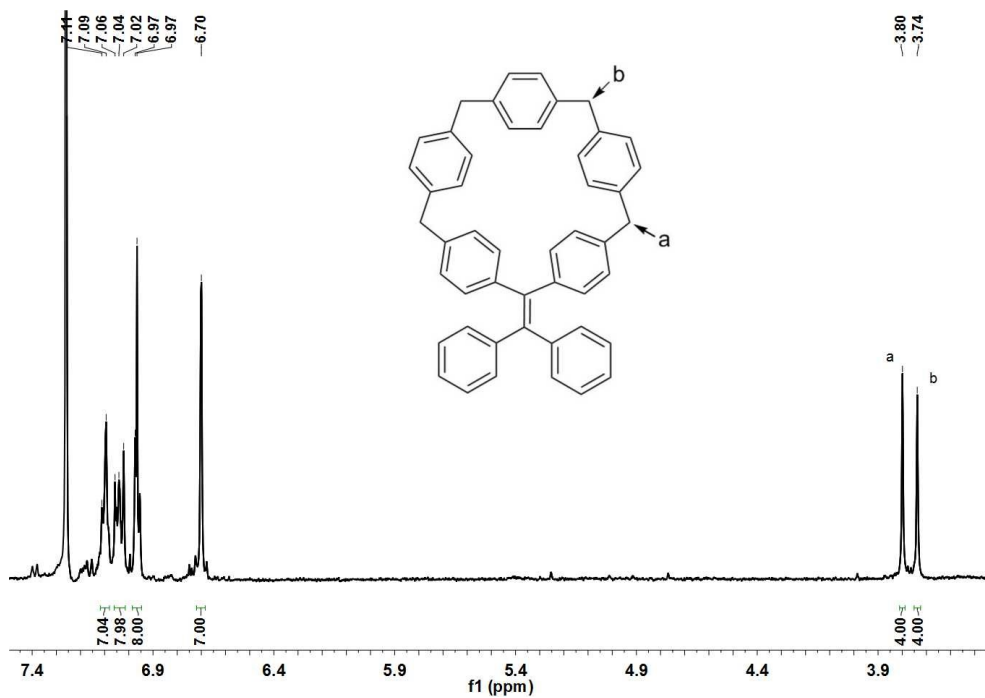
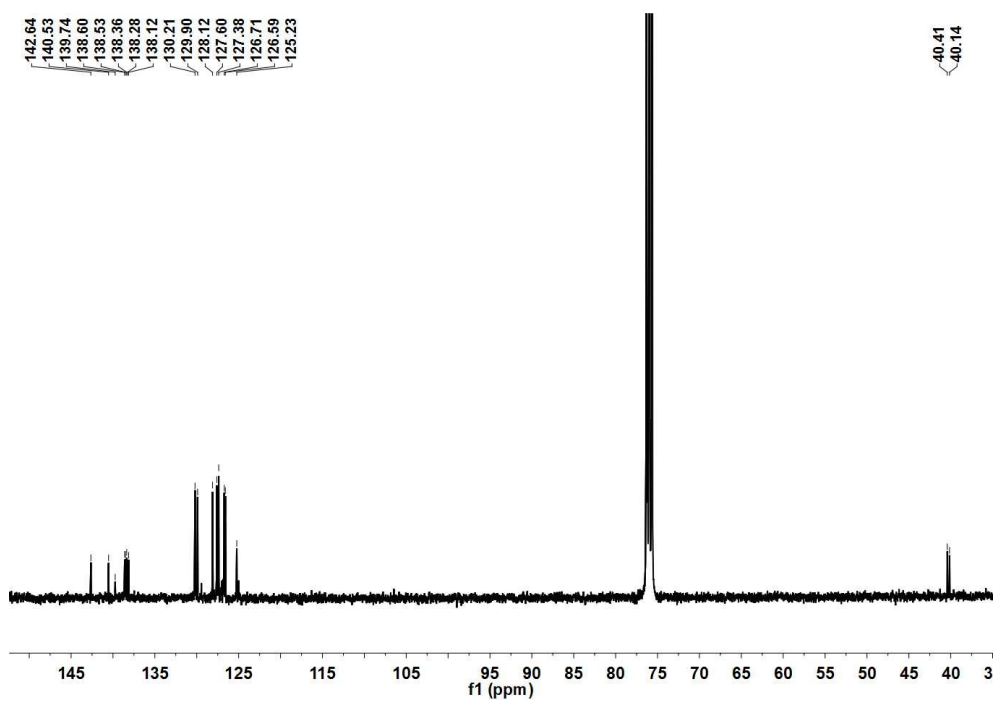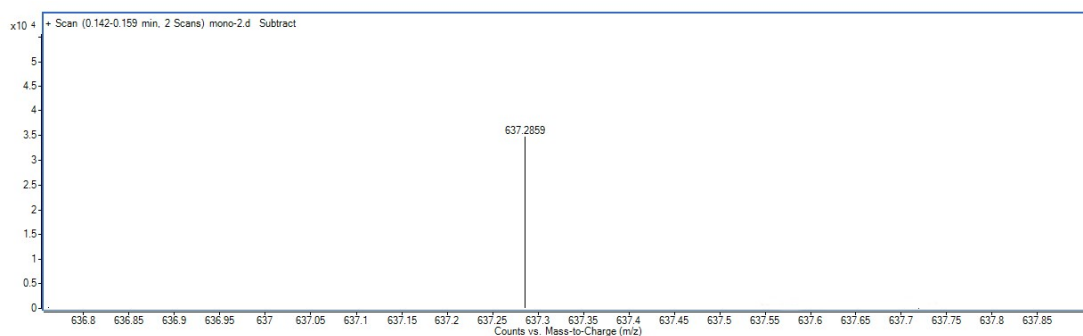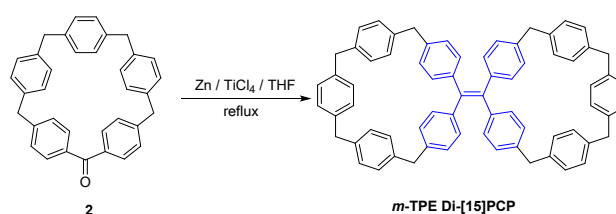**Fig. S7.** ^{1}H NMR spectrum of ***m*-TPE Mono-[1$_5$]PCP** in CDCl$_3$.

Fig. S8. ^{13}C NMR spectrum of ***m*-TPE Mono-[1$_5$]PCP** in CDCl$_3$.

Fig. S9. HR-ESI-MS data for *m*-TPE **Mono-[1$_5$]PCP** (Calculated [M+Na]$^+$: C$_{48}$H$_{38}$Na$^+$ = 637.2871, Found: 637.2859).

Scheme S5. Synthesis of compound *m*-TPE **Di-[1$_5$]PCP**.

To a solution of compound **2** (75 mg, 0.162 mmol) in of anhydrous THF (10 mL), zinc powder (423.86 mg, 6.48 mmol) was added in a 50 mL pressure-resistant bottle under N$_2$ protection. The mixture was cooled to –20 ˚C for 30 mins. Then, TiCl$_4$ (0.356 mL, 3.24 mmol) was added and the solution was refluxed overnight. The reaction was quenched by saturated NaHCO$_3$ solution (10 mL). After filtration, the solvent was removed under reduced pressure, the residue was dissolved in CH$_2$Cl$_2$ (200 mL), and washed with 1 M HCl (2 × 100 mL) and brine (2 × 100 mL). The organic phase was dried over anhydrous Na$_2$SO$_4$ and the solvent was removed under vacuum. Column chromatography (PE/ dichloromethane = 6/1~2/1, *v/v*, R$_f$ = 0.4) gave *m*-TPE **Di-[1$_5$]PCP** (50 mg, 0.0557 mmol, 34%) as a white solid. ^{1}H NMR (400 MHz, CDCl$_3$, 298 K) δ 7.03 (d, *J* = 7.9 Hz, 8H), 6.96 (m, 16H), 6.72 (s, 16H), 3.80 (s, 8H), 3.74 (s, 8H); ^{13}C NMR (100 MHz, CDCl$_3$, 298 K) δ 141.45, 139.60, 139.38, 139.17, 139.14, 130.81, 129.11, 128.61, 128.42, 127.74, 41.44, 41.21. HR-ESI-MS: m/z calcd. [M+Na]$^+$ 919.4280, found 919.4269.
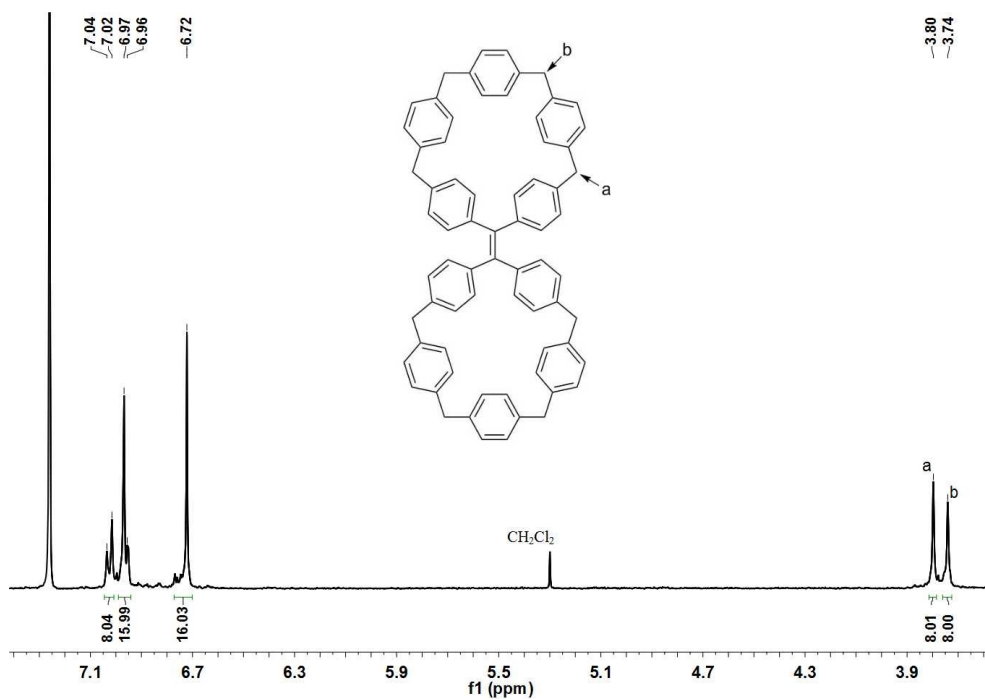
Fig. S10. ^{1}H NMR spectrum of ***m*-TPE Di-[1$_5$]PCP** in CDCl$_3$.
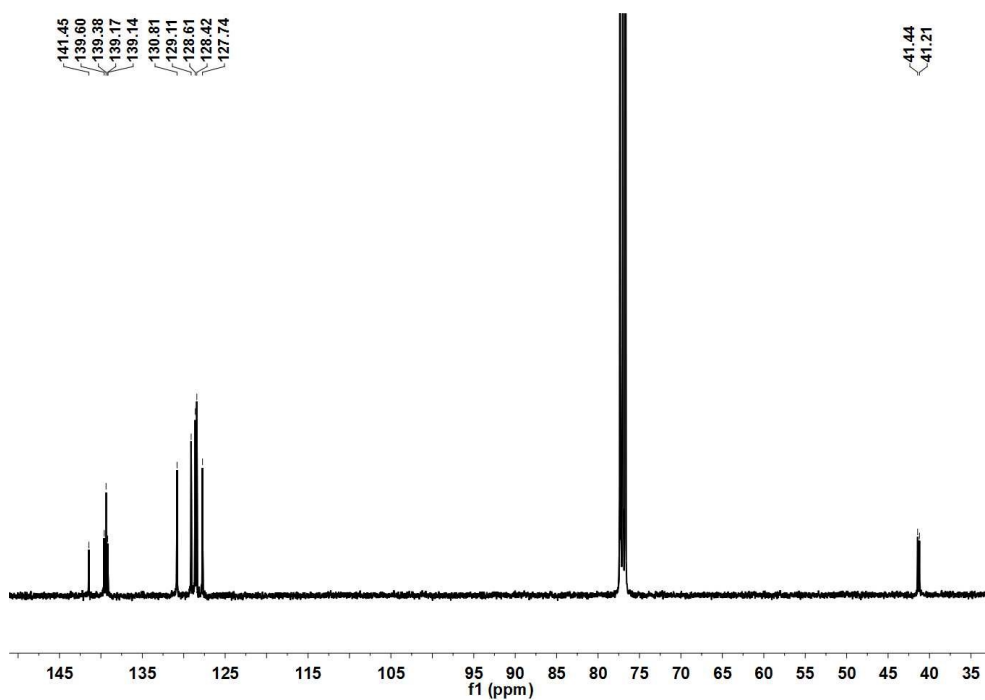
Fig. S11. ^{13}C NMR spectrum of ***m*-TPE Di-[1$_5$]PCP** in CDCl$_3$.
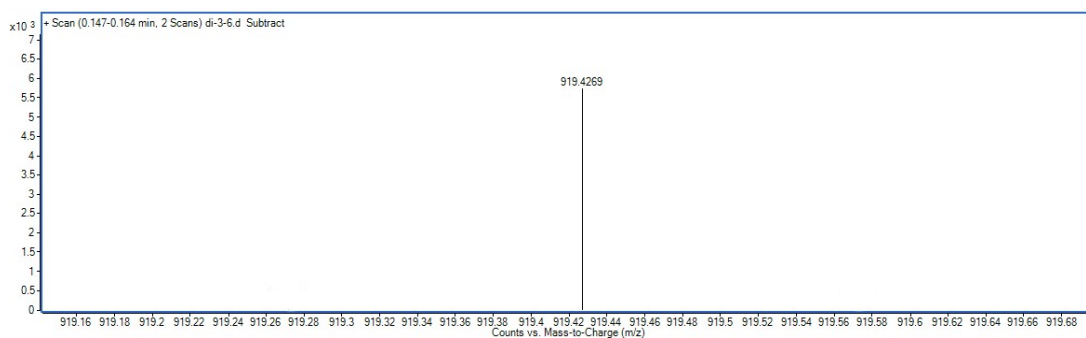
Fig. S12. HR-ESI-MS data for *m*-TPE **Di-[1$_5$]PCP** (Calculated [M+Na]$^+$: C$_{70}$H$_{56}$Na$^+$ = 919.4280, Found: 919.4269).

3. X-ray crystallography data of *m*-TPE Mono-[1$_5$]PCP and *m*-TPE Di-[1$_5$]PCP
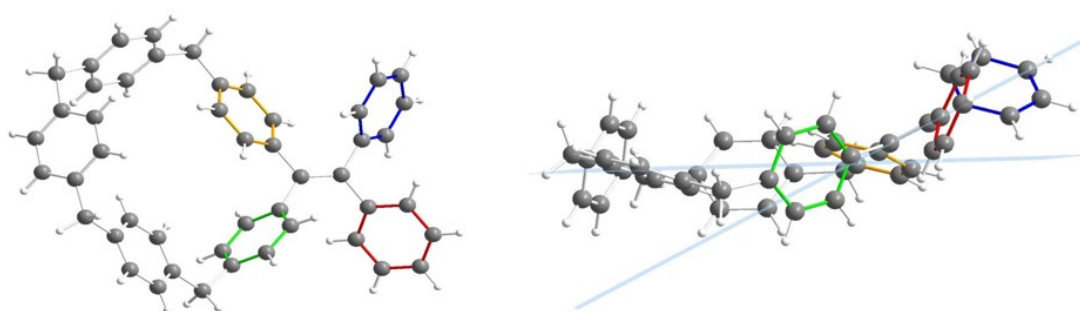
Fig. S13. Top and side view of crystal structures of *m*-TPE **Mono-[1$_5$] PCP**.

Table S1. Crystal data and structure refinement for *m*-TPE **Mono-[1$_5$] PCP** (CCDC: 2075493).

Empirical formula	C$_{48}$ H$_{38}$
Formula weight	614.78
Temperature	190(2) K
Wavelength	1.34139 Å
Crystal system	Monoclinic
Space group	*P*2$_1$
Unit cell dimensions	*a* = 11.7412(4) Å $\quad$ *a*= 90°.
	b = 9.4283(3) Å $\quad$ *b*= 97.3510(10)°.
	c = 16.2155(5) Å $\quad$ *g* = 90°.
Volume	1780.30(10) Å^3
Z	2
Density (calculated)	1.147 Mg/m^3
Absorption coefficient	0.310 mm^{-1}
F(000)	652
Crystal size	0.200 x 0.180 x 0.160 mm^3
Theta range for data collection	2.390 to 53.927°.
Index ranges	-13<=*h*<=14, -10<=*k*<=11, -19<=*l*<=19

Reflections collected	15832
Independent reflections	5921 [R(int) = 0.0353]
Completeness to theta = 53.594°	99.7 %
Absorption correction	None
Refinement method	Full-matrix least-squares on F^2
Data / restraints / parameters	5921 / 1 / 433
Goodness-of-fit on F^2	1.073
Final R indices [I>2sigma(I)]	R_1 = 0.0349, wR_2 = 0.0883
R indices (all data)	R_1 = 0.0391, wR_2 = 0.0953
Absolute structure parameter	2.8(7)
Extinction coefficient	n/a
Largest diff. peak and hole	0.348 and -0.169 e.Å^{-3}

Table S2. Atomic coordinates ($\times 10^4$)and equivalent isotropic displacement parameters (Å$^2 \times 10^3$) for *m*-TPE Mono-[1$_5$] PCP. U(eq) is defined as one third of the trace of the orthogonalized Uij tensor.

	x	y	z	U(eq)
C(1)	8119(2)	5138(2)	6664(1)	32(1)
C(2)	5086(2)	4748(3)	6791(1)	35(1)
C(3)	9162(2)	5293(3)	6361(1)	35(1)
C(4)	8055(2)	4722(2)	7480(1)	34(1)
C(5)	10194(2)	5032(3)	6861(1)	38(1)
C(6)	4551(2)	2872(3)	5795(1)	36(1)
C(7)	4373(2)	4219(3)	6115(1)	36(1)
C(8)	4389(2)	2936(2)	4233(1)	34(1)
C(9)	6018(2)	3956(3)	7157(1)	34(1)
C(10)	10991(2)	5258(3)	3858(2)	42(1)
C(11)	10792(2)	4037(3)	4293(2)	42(1)
C(12)	6914(2)	4604(3)	7784(1)	35(1)
C(13)	6169(2)	2596(3)	6856(2)	38(1)
C(14)	5440(2)	2057(3)	6194(1)	38(1)
C(15)	3698(2)	3270(3)	3498(2)	38(1)
C(16)	9477(2)	5071(3)	2635(1)	43(1)
C(17)	4161(2)	3748(3)	2808(2)	40(1)
C(18)	11277(2)	5232(3)	5610(2)	39(1)
C(19)	7564(2)	5959(3)	9073(1)	39(1)
C(20)	5335(2)	3916(3)	2821(1)	39(1)
C(21)	8712(2)	6143(3)	2787(2)	43(1)
C(22)	5565(2)	3111(3)	4247(2)	40(1)
C(23)	7101(2)	4726(3)	2204(1)	42(1)
C(24)	6695(2)	5122(3)	8530(1)	37(1)
C(25)	8082(2)	7154(3)	8777(2)	45(1)

C(26)	3881(2)	2386(3)	4988(2)	41(1)
C(27)	6027(2)	3587(3)	3554(2)	41(1)
C(28)	10132(2)	4584(3)	7671(2)	45(1)
C(29)	10940(2)	4020(3)	5155(2)	41(1)
C(30)	11483(2)	6443(3)	5171(2)	47(1)
C(31)	9090(2)	4432(3)	7974(1)	43(1)
C(32)	5568(2)	4930(3)	8846(1)	44(1)
C(33)	7866(2)	3673(3)	2043(2)	50(1)
C(34)	7544(2)	5972(3)	2573(2)	43(1)
C(35)	9035(2)	3844(3)	2256(2)	50(1)
C(36)	11343(2)	5232(3)	6545(2)	47(1)
C(37)	11349(2)	6452(3)	4305(2)	49(1)
C(38)	10747(2)	5266(4)	2914(2)	53(1)
C(39)	7863(2)	5583(4)	9906(2)	54(1)
C(40)	5089(2)	6052(3)	9242(2)	53(1)
C(41)	5817(2)	4488(3)	2060(2)	52(1)
C(42)	8886(3)	7921(4)	9278(2)	64(1)
C(43)	4977(3)	3643(4)	8779(2)	60(1)
C(44)	8675(3)	6347(5)	10408(2)	74(1)
C(45)	4040(3)	5906(5)	9541(2)	73(1)
C(46)	3930(3)	3508(5)	9077(2)	80(1)
C(47)	3458(3)	4639(5)	9453(2)	83(1)
C(48)	9192(3)	7497(5)	10099(2)	82(1)
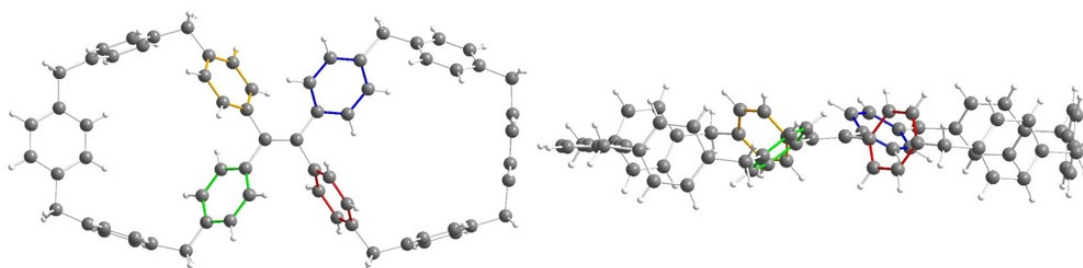
Fig. S14. Top and side view of crystal structures of *m*-TPE Di-[1₅]PCP.

Table S3. Crystal data and structure refinement for *m*-TPE Di-[1₅]PCP (CCDC: 2075494).

Empirical formula	$C_{70} H_{56}$	
Formula weight	897.14	
Temperature	296.15 K	
Wavelength	0.71073 Å	
Crystal system	Triclinic	
Space group	*P*-1	
Unit cell dimensions	*a* = 12.0998(10) Å	*a*= 91.781(3)°.
	b = 12.6272(12) Å	*b*= 90.797(3)°.
	c = 17.4091(13) Å	*g* = 99.727(3)°.

Volume	2619.9(4) Å^3	
Z	2	
Density (calculated)	1.137 Mg/m^3	
Absorption coefficient	0.064 mm^{-1}	
F(000)	952	
Crystal size	0.12 x 0.12 x 0.1 mm^3	
Theta range for data collection	1.980 to 27.554°.	
Index ranges	-15<=h<=15, -13<=k<=16, -22<=l<=22	
Reflections collected	24807	
Independent reflections	11975 [R(int) = 0.0838]	
Completeness to theta = 25.242°	99.3 %	
Absorption correction	Semi-empirical from equivalents	
Max. and min. transmission	0.7456 and 0.6341	
Refinement method	Full-matrix least-squares on F^2	
Data / restraints / parameters	11975 / 0 / 631	
Goodness-of-fit on F^2	1.019	
Final R indices [I>2sigma(I)]	R_1 = 0.0778, wR_2 = 0.1835	
R indices (all data)	R_1 = 0.1779, wR_2 = 0.2389	
Extinction coefficient	n/a	
Largest diff. peak and hole	0.291 and -0.177 e.Å^{-3}	

Table S4. Atomic coordinates ($\times 10^4$) and equivalent isotropic displacement parameters (Å$^2 \times 10^3$) for **m-TPE Di-[1$_5$]PCP**. U(eq) is defined as one third of the trace of the orthogonalized Uij tensor.

	x	y	z	U(eq)
C(68)	4625(2)	5482(2)	3246(2)	43(1)
C(33)	3647(3)	2565(2)	3916(2)	46(1)
C(1)	3829(2)	3762(2)	3852(2)	42(1)
C(36)	4471(2)	4289(2)	3306(2)	42(1)
C(67)	3758(3)	6003(2)	3040(2)	49(1)
C(2)	3227(2)	4317(2)	4443(2)	44(1)
C(7)	3659(3)	5289(2)	4811(2)	48(1)
C(69)	5683(3)	6108(2)	3364(2)	49(1)
C(37)	5055(2)	3769(2)	2691(2)	45(1)
C(70)	5856(3)	7204(3)	3276(2)	54(1)
C(66)	3950(3)	7112(2)	2942(2)	50(1)
C(65)	4984(3)	7723(2)	3051(2)	49(1)
C(42)	5568(3)	2868(2)	2766(2)	51(1)
C(61)	5785(3)	9173(2)	2168(2)	50(1)
C(6)	3046(3)	5753(2)	5348(2)	54(1)

C(30)	3236(3)	328(2)	4115(2)	52(1)
C(26)	2248(3)	-1135(2)	4926(2)	52(1)
C(41)	6073(3)	2446(3)	2156(2)	54(1)
C(31)	2900(3)	755(2)	3456(2)	52(1)
C(34)	3999(3)	2131(2)	4577(2)	56(1)
C(23)	853(3)	-1482(2)	6200(2)	56(1)
C(64)	5200(3)	8924(2)	2909(2)	57(1)
C(9)	839(3)	5061(3)	6753(2)	61(1)
C(24)	2007(3)	-1405(2)	6273(2)	60(1)
C(25)	2694(3)	-1241(2)	5648(2)	56(1)
C(5)	1977(3)	5283(2)	5550(2)	60(1)
C(40)	6112(3)	2882(3)	1439(2)	56(1)
C(35)	3804(3)	1032(3)	4674(2)	60(1)
C(32)	3102(3)	1869(3)	3350(2)	52(1)
C(44)	7230(3)	3251(3)	236(2)	60(1)
C(27)	1100(3)	-1237(3)	4851(2)	65(1)
C(38)	5108(3)	4214(3)	1968(2)	58(1)
C(3)	2161(3)	3830(3)	4661(2)	62(1)
C(18)	416(3)	461(3)	6912(2)	61(1)
C(12)	-28(4)	3508(3)	7803(2)	65(1)
C(28)	412(3)	-1406(3)	5477(2)	64(1)
C(14)	-281(3)	4532(3)	6698(2)	65(1)
C(58)	6917(3)	9597(3)	785(2)	64(1)
C(19)	-11(3)	-491(3)	7250(2)	60(1)
C(13)	-684(3)	3775(3)	7214(2)	66(1)
C(20)	-602(3)	-429(3)	7918(2)	63(1)
C(16)	-304(3)	1501(3)	7914(2)	65(1)
C(51)	8489(3)	6901(3)	-916(2)	64(1)
C(56)	9202(3)	7586(3)	-436(2)	70(1)
C(47)	8236(3)	4912(3)	-703(2)	65(1)
C(21)	-745(3)	545(3)	8236(2)	68(1)
C(29)	2980(3)	-873(2)	4244(2)	67(1)
C(39)	5614(3)	3775(3)	1362(2)	65(1)
C(17)	277(3)	1448(3)	7235(2)	65(1)
C(10)	1477(3)	4820(3)	7352(2)	72(1)
C(45)	6892(3)	3311(3)	-505(2)	71(1)
C(54)	7879(4)	8808(3)	-313(2)	69(1)
C(62)	6940(3)	9418(3)	2152(2)	70(1)
C(55)	8903(4)	8525(3)	-138(2)	72(1)
C(60)	5220(3)	9183(3)	1490(2)	69(1)
C(49)	8094(3)	4047(3)	514(2)	70(1)

C(4)	1554(3)	4301(3)	5199(2)	70(1)
C(48)	8590(3)	4861(3)	58(2)	74(1)
C(46)	7394(3)	4125(3)	-969(2)	72(1)
C(63)	7503(3)	9625(3)	1471(2)	72(1)
C(59)	5781(3)	9380(3)	809(2)	74(1)
C(8)	1319(3)	5803(3)	6138(2)	78(1)
C(22)	136(3)	-1578(3)	6903(2)	78(1)
C(50)	8747(4)	5815(3)	-1198(2)	79(1)
C(43)	6675(3)	2420(3)	769(2)	75(1)
C(52)	7476(4)	7188(3)	-1110(2)	77(1)
C(57)	7532(4)	9820(3)	34(2)	83(1)
C(53)	7179(4)	8153(4)	-812(2)	79(1)
C(11)	1065(4)	4061(3)	7871(2)	78(1)
C(15)	-438(4)	2582(3)	8299(2)	90(1)

4. Mechanical force and solvent fumigation change fluorescence

(a) *m*-TPE Mono-[1₅]PCP

(b) *m*-TPE Di-[1₅]PCP

Before grinding   5 min   10 min   methanol fuming
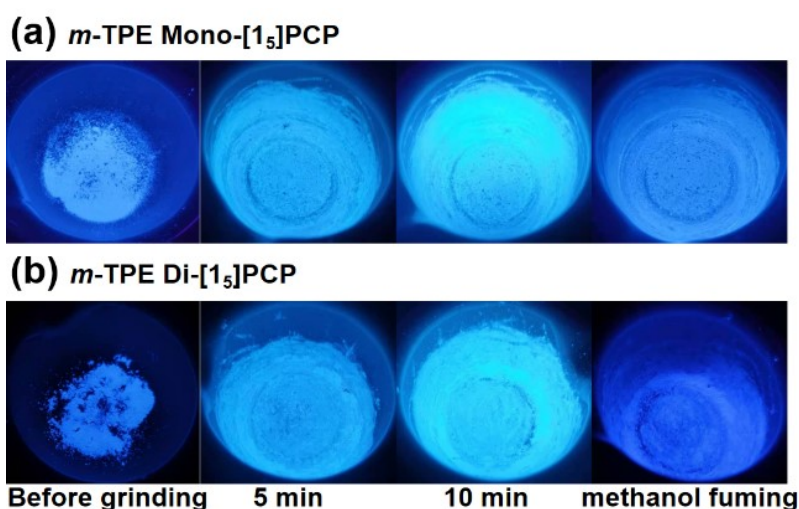
Fig. S15. The photographs of *m*-**Di Mono-[1$_5$]PCP** and *m*-**TPE Di-[1$_5$]PCP** after grinding and exposure to methanol vapour.

5. Photophysical properties

5.1 fluorescence spectra

Samples with different water content were prepared by adding 0.03 mL of the sample solution in THF (1×10^{-3} M) to premixed THF/H_2O (2.97 mL, with appropriate ratio). The fluorescence intensity of the three compounds (**TPE**, *m*-**TPE Mono-[1$_5$]PCP**, and *m*-**TPE Di-[1$_5$]PCP**) all increased with the increase of water content, verifying that the compounds with TPE structure all have AIE effect (**Fig. S16-S21**). **TPE** starts emitting from 93% of

water content, whereas the fluorescence intensity of *m*-TPE Mono-[1$_5$]PCP and *m*-TPE Di-[1$_5$]PCP becomes apparently at 90% and 70% of water content, respectively. In addition, the fluorescence gradually shows blue shifts as the solution becomes more aggregated. Solid state fluorescence demonstrated further blue shifts (**Fig. S22-S23**).
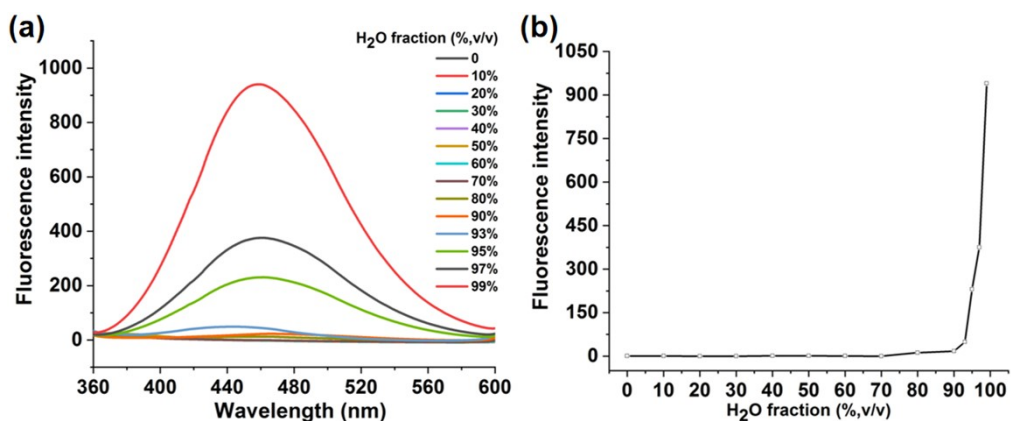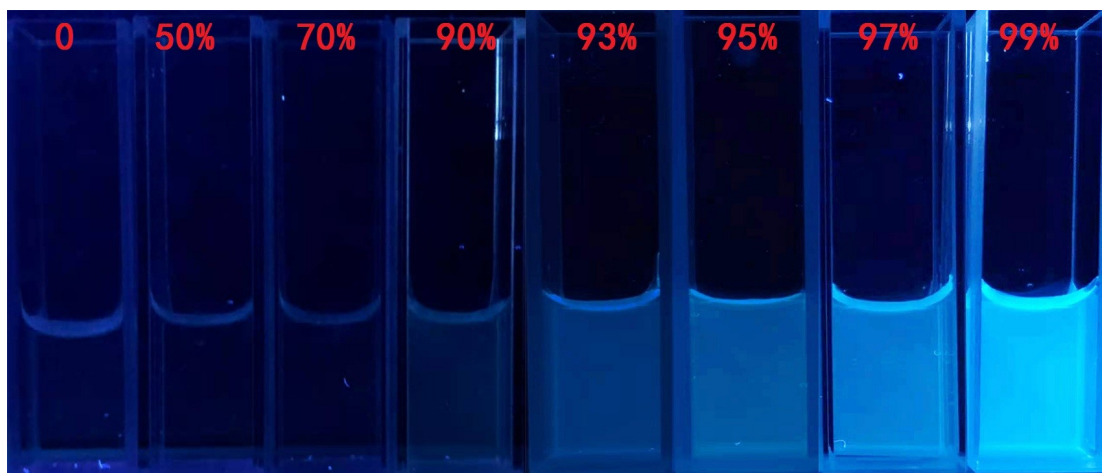

Fig. S16. (a) Fluorescence spectra of **TPE** (1×10^{-5} M) and (b) Plot of the highest fluorescence intensity in different THF/H$_2$O mixed solutions.
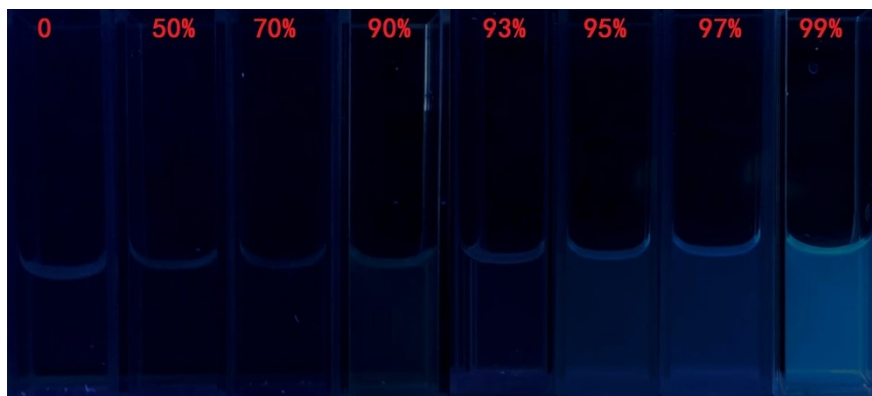
Fig. S17. Images of **TPE** in THF/H$_2$O mixed solutions (from left to right: 0%, 50%, 70%, 90%, 93%, 95%, 97%, and 99%).
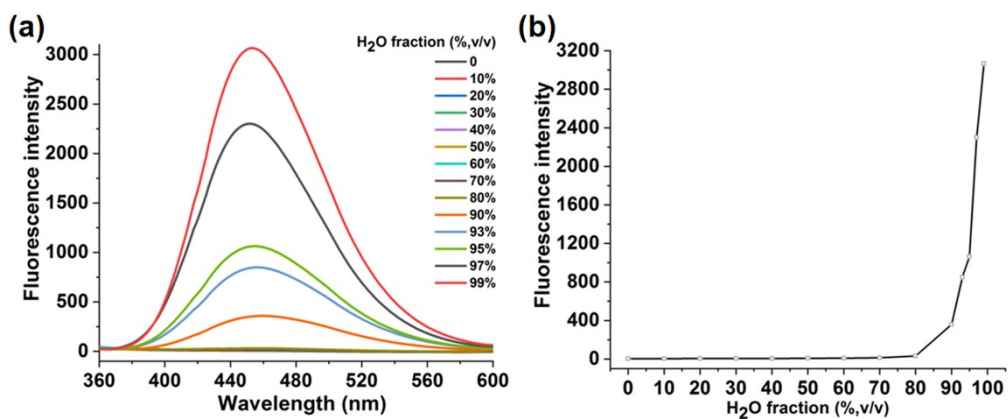
Fig. S18. (a) Fluorescence spectra of *m*-TPE Mono-[1$_5$]-PCP (1 × 10^{-5} M) and (b) Plot of the highest fluorescence intensity in different THF/H$_2$O mixed solutions.

Fig. S19. Images of *m*-TPE Mono-[1$_5$]-PCP in THF/H$_2$O mixed solutions (from left to right: 0%, 50%, 70%, 90%, 93%, 95%, 97%, and 99%).
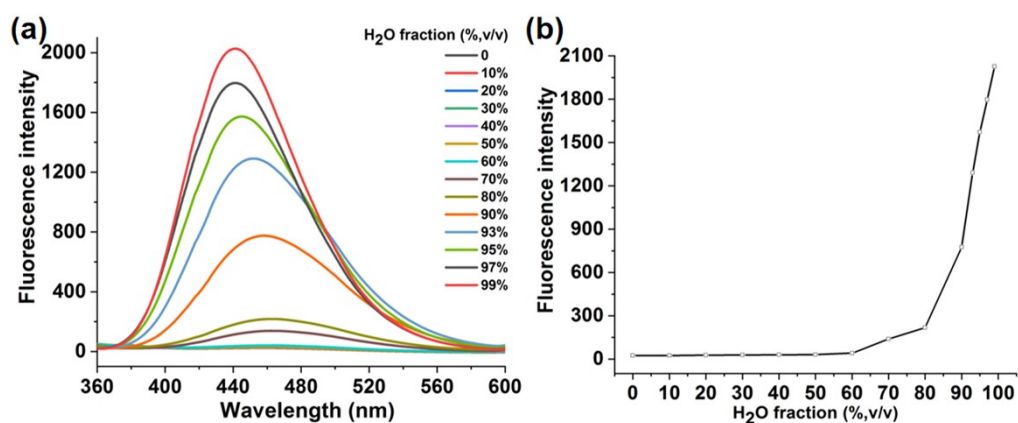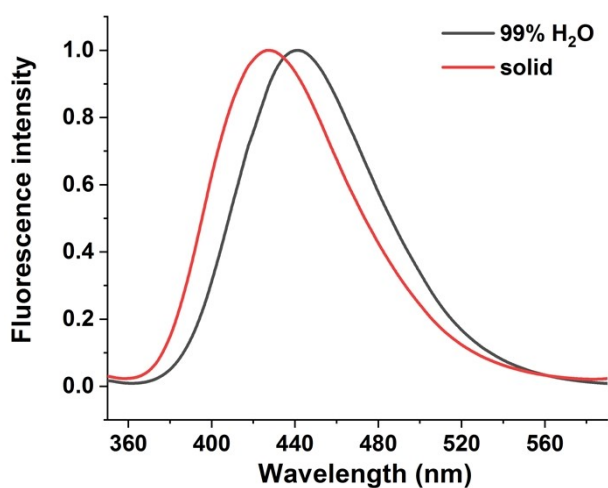

Fig. S20. (a) Fluorescence spectra of *m*-TPE Di-[1$_5$]-PCP (1 × 10^{-5} M) and (b) Plot of the highest fluorescence intensity in different THF/H$_2$O mixed solutions.
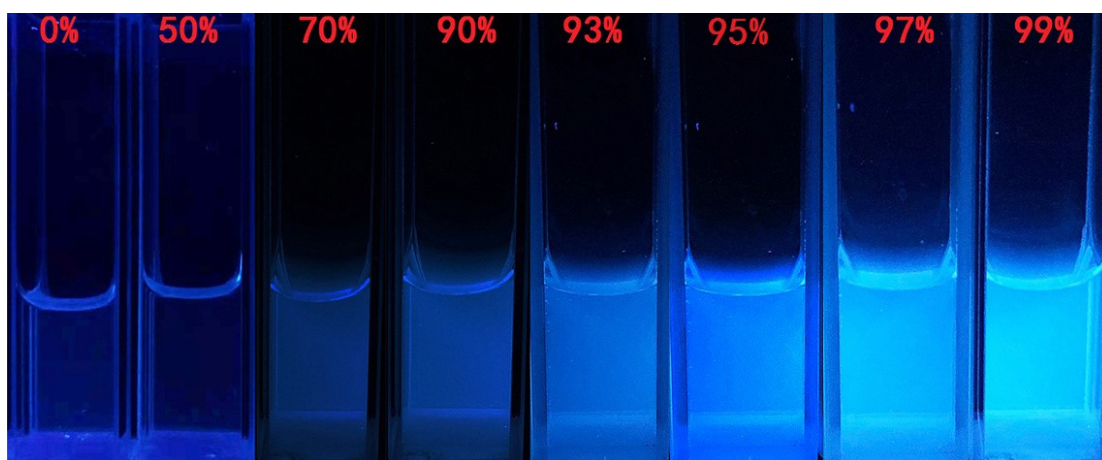
Fig. S21. Images of *m*-TPE Di-[1$_5$]-PCP in THF/H$_2$O mixed solutions (from left to right: 0%, 50%, 70%, 90%, 93%, 95%, 97%, and 99%).
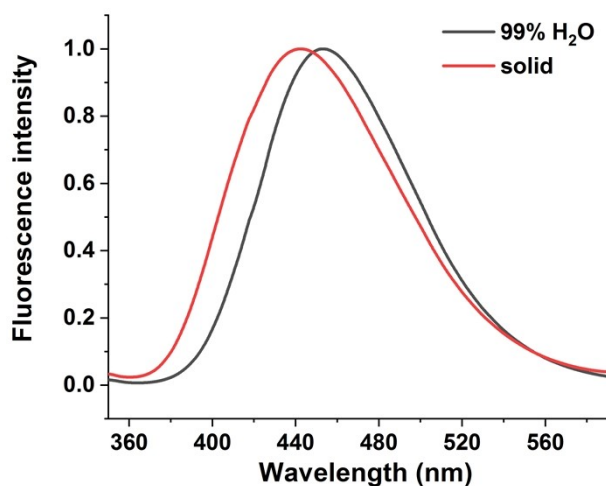
Fig. S22. Normalized fluorescence spectra of **m-TPE Mono-[1$_5$] PCP** (λ_{ex} = 310 nm) in 99% H_2O solution and in solid state.

Fig. S23. Normalized fluorescence spectra of **m-TPE Di-[1$_5$] PCP** (λ_{ex} = 310 nm) in 99% H_2O solution and in solid state.

5.2 Fluorescence lifetime measurements
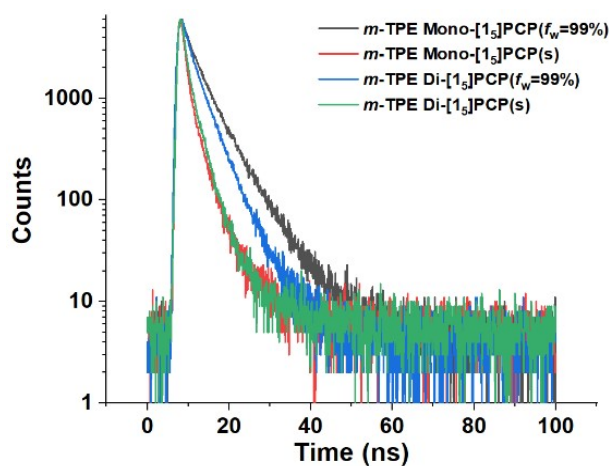
Fig. S24. Fluorescence decay profiles of **m-TPE Mono-[1$_5$]PCP** (f_w = 99%, 1 × 10^{-5} M, black line), **m-**

TPE Mono-[1₅]PCP(s) (red line), *m*-TPE Di-[1₅]PCP (f_w = 99%, 1 × 10⁻⁵ M, blue line), *m*-TPE Mono-[1₅]PCP(s) (green line).
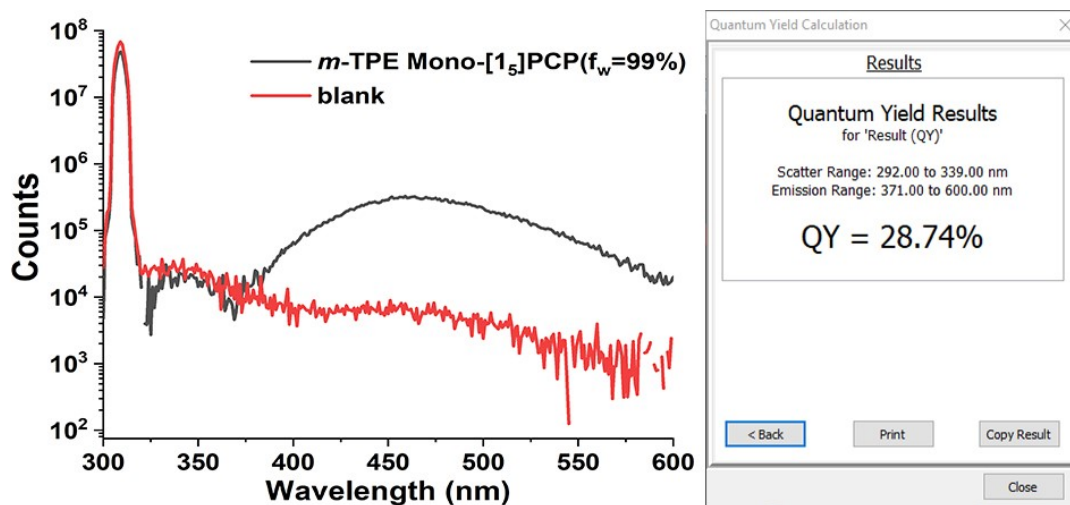
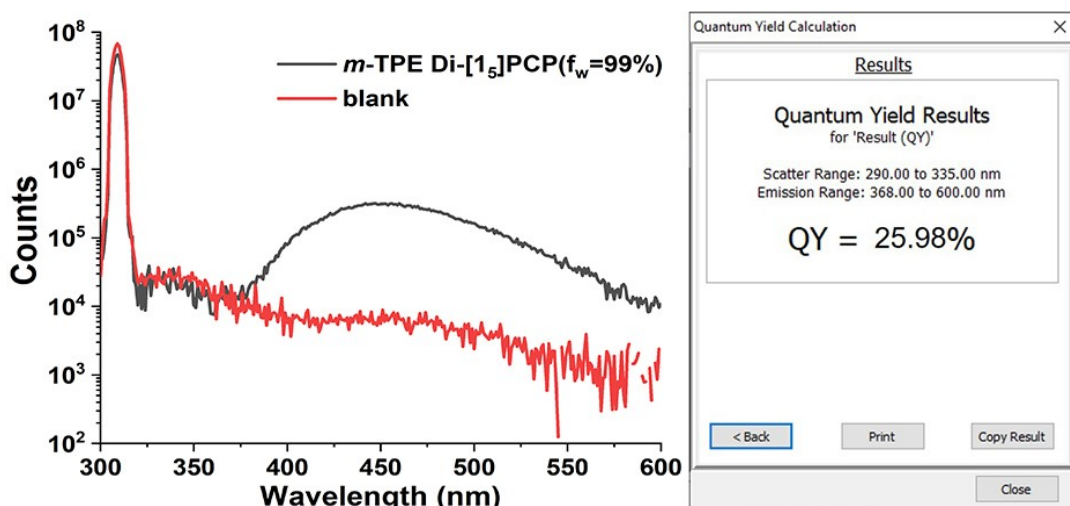**Fig. S25**. Quantum yield of *m*-TPE Mono-[1₅]PCP (f_w=99%).

Fig. S26. Quantum yield of *m*-TPE Di-[1₅]PCP (f_w=99%).

Table S5. Fluorescence decay profiles and the radiative and non-radiative rate constants of *m*-TPE Mono-[1₅]PCP (f_w = 99%, 1 × 10⁻⁵ M), *m*-TPE Mono-[1₅]PCP (solid), *m*-TPE Di-[1₅]PCP (f_w = 99%, 1 × 10⁻⁵ M), *m*-TPE Mono-[1₅]PCP (solid). (Monitored at 460 nm (*m*-TPE Mono-[1₅]PCP) and 440 nm (*m*-TPE Di-[1₅]PCP) upon excitation at 310 nm).

Sample	τ_1/ ns	RW_1[%]	τ_2/ ns	RW_2[%]	τ/ ns	χ^2	Φ_f	$k_r \times 10^{-7}$ (s⁻¹)	$k_{nr} \times 10^{-7}$ (s⁻¹)
m-TPE Mono-[1₅]PCP (f_w = 99%)	2.43	28.29	5.99	71.71	4.98	1.17	0.29	5.82	14.26
m-TPE Mono-[1₅]PCP (solid)	2.39	65.50	6.54	34.50	3.82	1.29	0.15	3.93	22.25
m-TPE Di-[1₅]PCP (f_w = 99%)	2.39	39.83	4.70	60.17	3.78	1.19	0.26	6.88	19.58

m-TPE Di-[1$_5$]PCP (solid)	2.24	73.61	5.00	26.39	2.97	1.20 2	0.1 7	5.72	27.95

5.3 Fluorescence quenching experiments

A series of metal chloride salts (Ba^{2+}, Ca^{2+}, Cu^{2+}, Fe^{2+}, Mn^{2+}, Fe^{3+}, Al^{3+}, Mg^{2+}, Ni^{2+}, Zn^{2+} and Pb^{2+}) were added to the three compounds bearing TPE units and fluorescence intensity was measured (**Fig. S27-S29**). It can be concluded that the quenching effect of Ni^{2+} on ***m*-TPE Mono-[1$_5$]PCP** and ***m*-TPE Di-[1$_5$]PCP** is very good, whereas TPE shows little quenching effect on most ions. Therefore, we investigated the quenching effect of Ni^{2+} ion on ***m*-TPE Mono-[1$_5$]PCP** and ***m*-TPE Di-[1$_5$]PCP** by titration measurements (**Fig. S30-S33**).
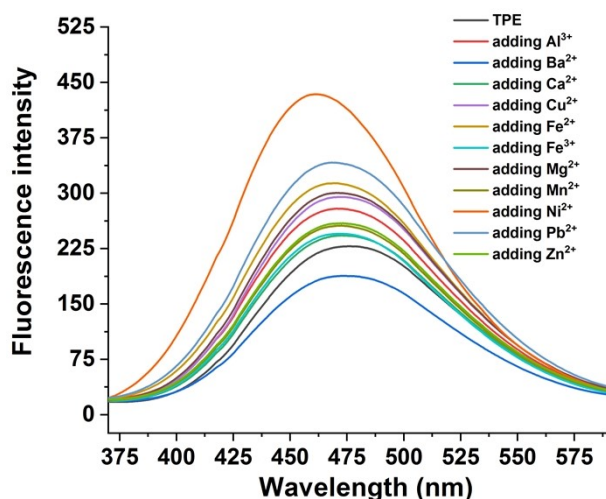

Fig. S27. Fluorescence quenching spectra of 5/95 THF/H$_2$O mixture of TPE (1 × 10^{-5} M , λ_{ex} = 310 nm) upon addition of 10 equiv. of various metal ions.
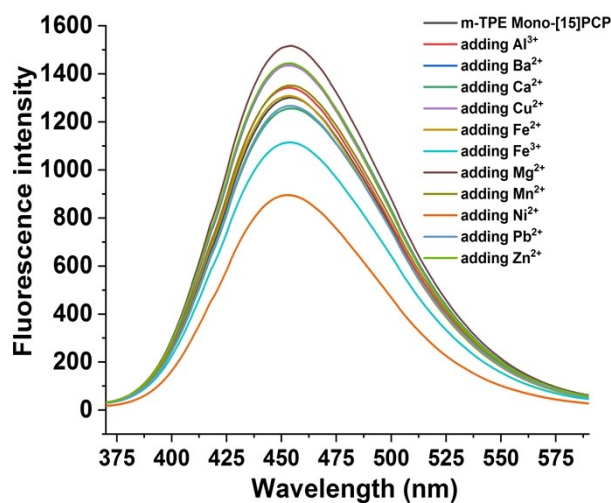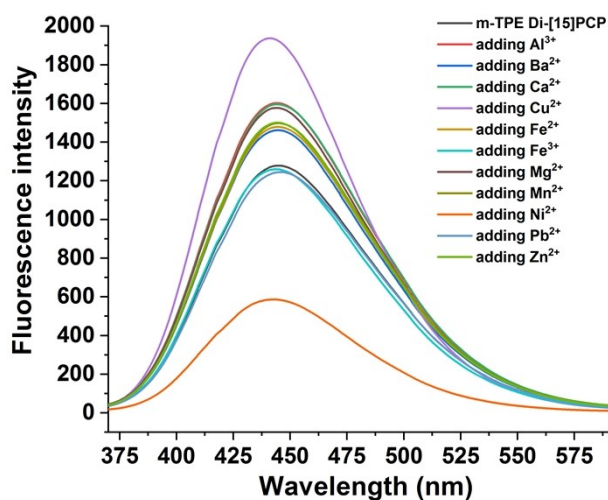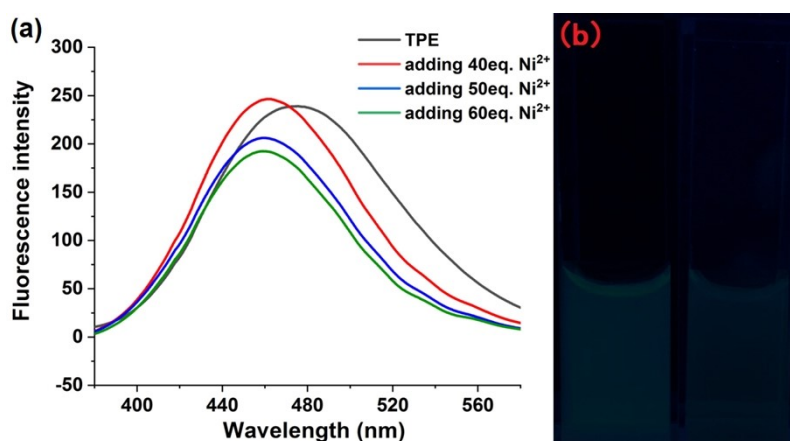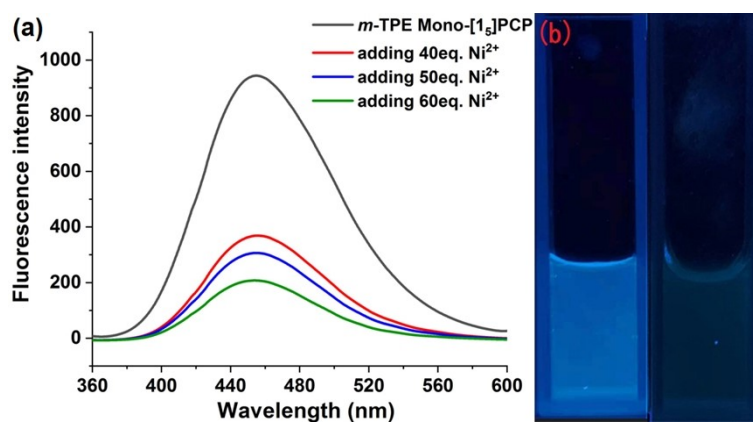

Fig. S28. Fluorescence quenching spectra of 5/95 THF/H$_2$O mixture of ***m*-TPE Mono-[1$_5$] PCP** (1 × 10^{-5} M) upon addition of 10 equiv. of various metal ions.
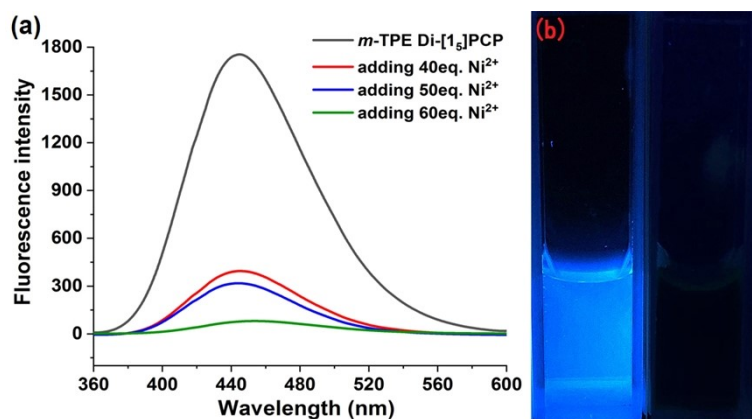
Fig. S29. Fluorescence quenching spectra of 5/95 THF/H$_2$O mixture of *m*-TPE Di-[1$_5$] PCP (1×10^{-5} M , λ_{ex} = 310 nm) upon addition of 10 equiv. of various metal ions.


Fig. S30. (a) Fluorescence quenching spectra of **TPE** (1×10^{-5} M in THF/H$_2$O =5:95, λ_{ex} = 310 nm,) upon addition of Ni^{2+} (40, 50, and 60 equiv.) and (b) the images of sample before (left) and after (right) adding Ni^{2+} under 365 nm irradiation.

Fig. S31. (a) Fluorescence quenching spectra of *m*-TPE Mono-[1$_5$] PCP (1×10^{-5} M in THF/H$_2$O =5:95, λ_{ex} = 310 nm) upon addition of Ni^{2+} (40, 50 and 60 equiv.) and (b) the images of sample before (left) and after (right) adding Ni^{2+} under 365 nm irradiation.

Fig. S32. (a) Fluorescence quenching spectra of **m-TPE Di-[1$_5$] PCP** (1×10^{-5} M in THF/H$_2$O =5:95, λ_{ex} = 310 nm) upon addition of Ni^{2+} (40, 50, and 60 equiv.) and (b) the images of sample before (left) and after (right) adding Ni^{2+} under 365 nm irradiation.
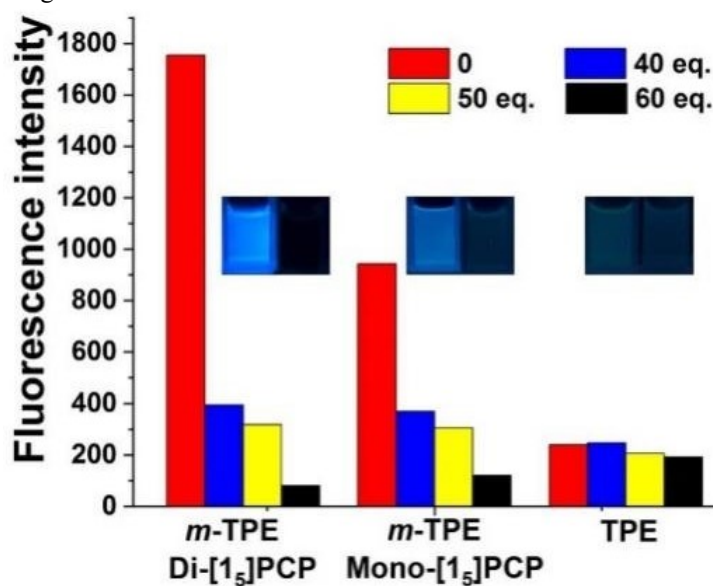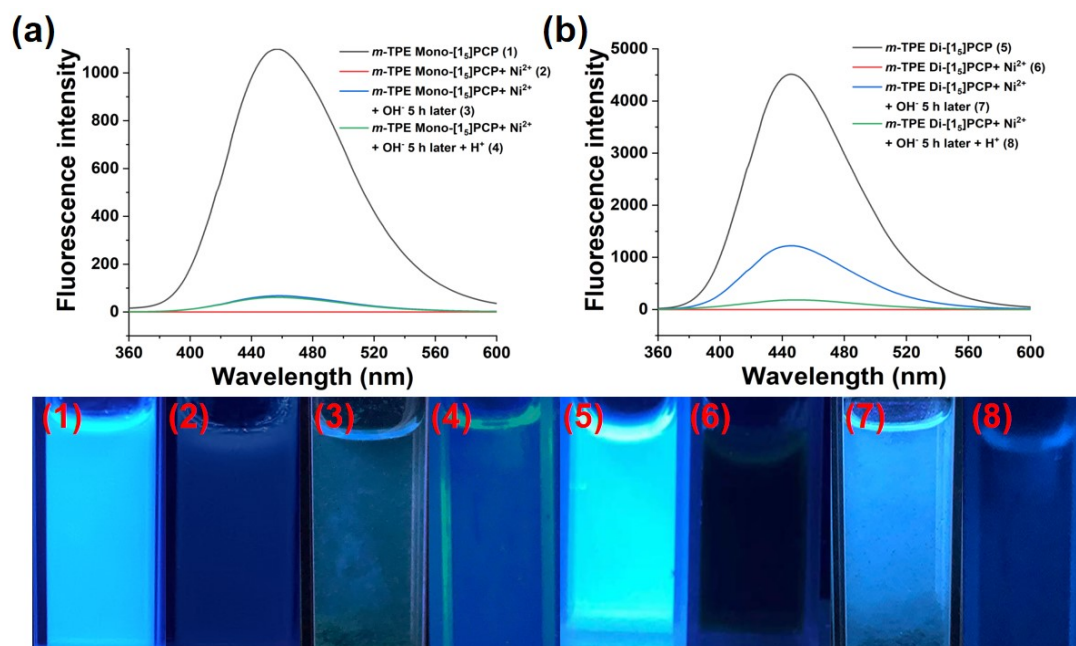

Fig. S33. Plot of highest fluorescence intensity of **m-TPE Di-[1$_5$]PCP**, **m-TPE Di-[1$_5$]PCP**, and TPE in 95:5 H$_2$O/THF mixtures upon addition of 40, 50 and 60 equiv. Ni^{2+} (Insets are the images of samples before and after adding 60 equiv. Ni^{2+} under 365 nm irradiation).

5.4 pH-Responsive fluorescence tuning process with NaOH and HCl

Fig. S34. (a) Fluorescence spectra and images of (1) *m*-TPE Mono-[1$_5$]-PCP (1 × 10^{-4} M in THF/H$_2$O = 5/95), (2) Adding NiCl$_2$ to (1), (3) Adding NaOH to (2), (4) Adding HCl to (3); (b) Fluorescence spectra and images of (5) *m*-TPE Di-[1$_5$]-PCP (1 × 10^{-4} M in THF/H$_2$O = 5/95), (6) Adding NiCl$_2$ to (5); (7) Adding NaOH to (6), (8) Adding HCl to (7).

6. TEM images of *m*-TPE Mono-[1$_5$]PCP and *m*-TPE Di-[1$_5$]PCP
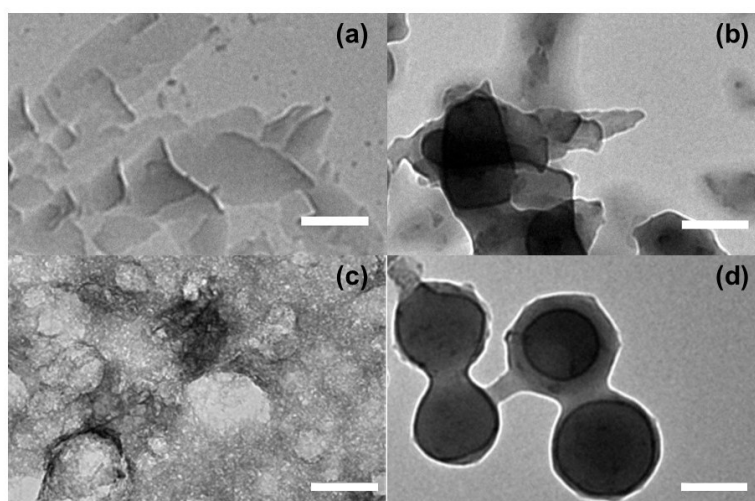
Fig. S35. TEM images of 1 × 10^{-5} M (a) *m*-TPE Mono-[1$_5$]PCP; (b) *m*-TPE Di-[1$_5$]PCP; (c) *m*-TPE Mono-[1$_5$]PCP with the addition of 10 equiv. Ni^{2+} ions; and (d) *m*-TPE Di-[1$_5$]PCP with the addition of 10 equiv. Ni^{2+} ions in 5/95 THF/H$_2$O solution. Scale bar: 200 nm.

7. Theoretical calculations

Energy minimized structure of the synthesized molecules were achieved using Gaussian 09 package.[S3] Optimization at ground state for *m*-TPE Mono-[1₅]PCP and *m*-TPE Di-[1₅]PCP were achieved using density functional theory employing B3LYP hybrid exchange functional[S4,S5] with 6-31G (d, p)[S6,S7] basis set. Similar functional and basis set were adopted to estimate the energy transitions at the excited state. Selection of the functional and the basis set was in line with the previous numerous benchmarks that better validates with great accuracy in estimating ground and transition states. Ground state frequency analysis resulting in the absence of negative frequency clearly validates the achieved optimized structure at the ground state corresponds to a true local minimum. All the geometry optimizations were carried in vacuum media and without any constraints on the geometrical parameters.
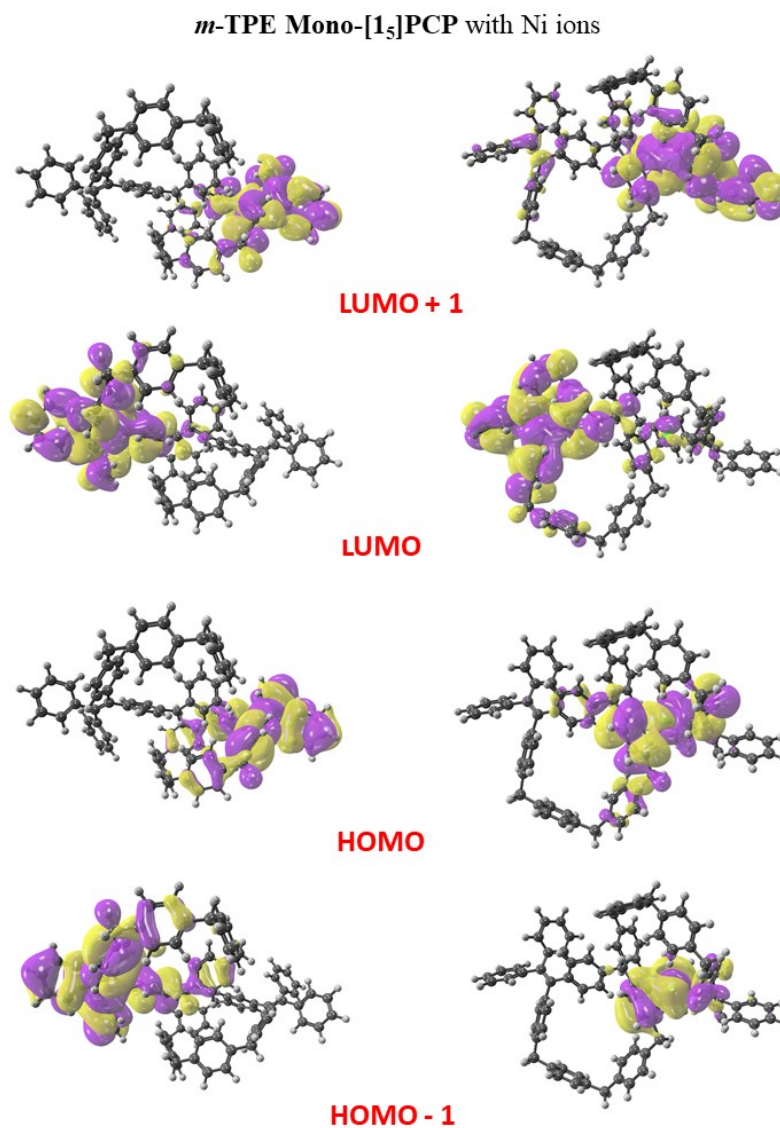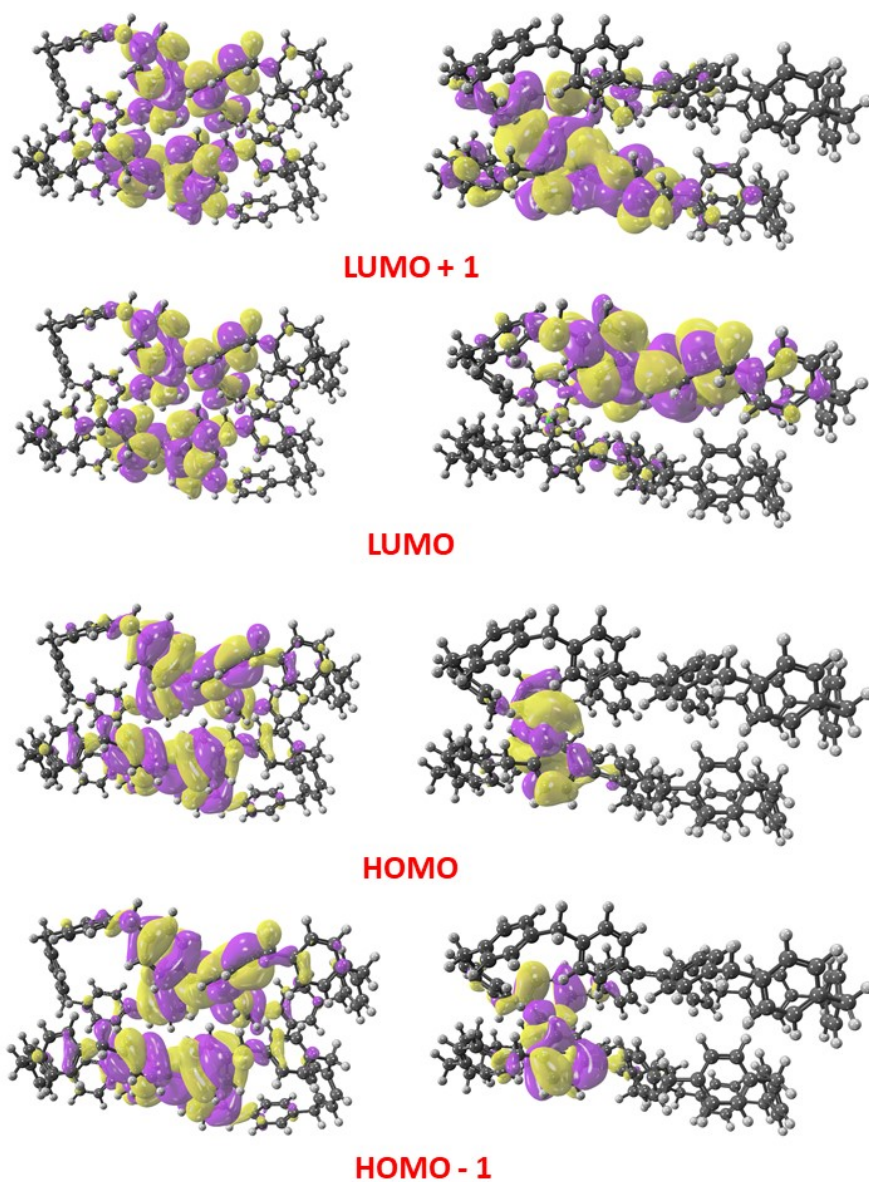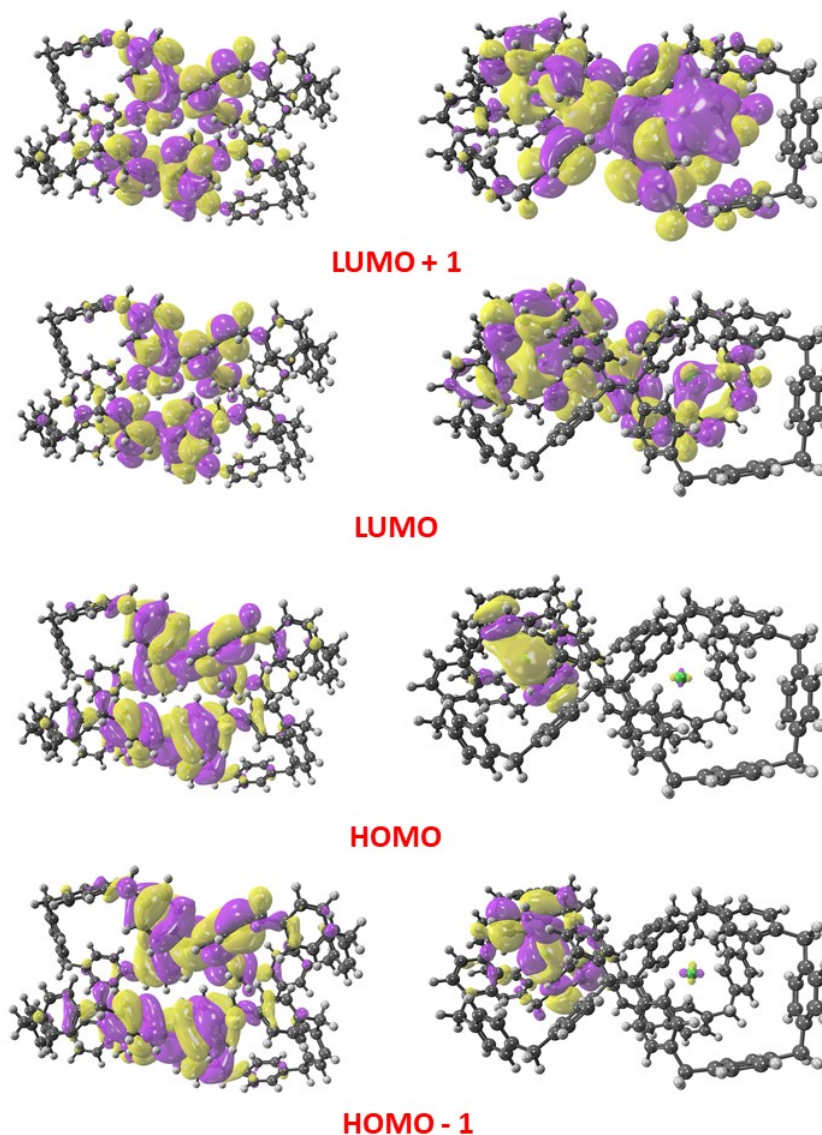
m-TPE Mono-[1₅]PCP with Ni ions

Fig. S36. Electronic orbital density of *m*-TPE Mono-[1₅]PCP fluorophore with the addition of Ni²⁺ ion.

m-TPE Di-[1₅]PCP + Single Ni ion

LUMO + 1

LUMO

HOMO

HOMO - 1

Fig. S37. Electronic orbital density of *m*-TPE Di-[1₅]PCP fluorophore with the addition of single Ni^{2+} ion.

m-TPE Di-[1₅]PCP + Double Ni ion

LUMO + 1

LUMO

HOMO

HOMO - 1

Fig. S38. Electronic orbital density of *m*-TPE **Di-[1₅]PCP** fluorophore with the addition of double Ni^{2+} ion.

Further analysis of the structures was performed by calculated electronic transition spectra. *m*-TPE **Mono-[1₅]PCP** and *m*-TPE **Di-[1₅]PCP** exhibited a transition at 342 and 340 nm, that can be attributed to the intermolecular charge transfer occurring within the dimer. Upon addition of Ni ions to *m*-TPE **Mono-[1₅]PCP**, the calculated electronic transitions were significantly redshifted to 453 and 554 nm, respectively (Fig. S39a). *m*-TPE **Di-[1₅]PCP** exhibited three peaks at 475, 583 and 666 nm upon addition of single and double Ni ions as shown in Fig. S39b. However, such well resolved redshifted spectra with fine resolution could not be observed in experimental UV-vis studies (Fig. S40). The new charge transfer band might be buried under the Ni^{2+} absorption at 460−600 nm. Interestingly, peak

broadening at lower wavelength upon addition of Ni^{2+} reveals an interaction between the host and the Ni-ions. Furthermore, the molecular absorption coefficient computed for the free host is greatly larger in comparison with that of the complexation. Such lower absorption energy of Ni^{2+} complex signifies the phenomenon of emission quenching brought about by metal to ligand charge transfer in the system.
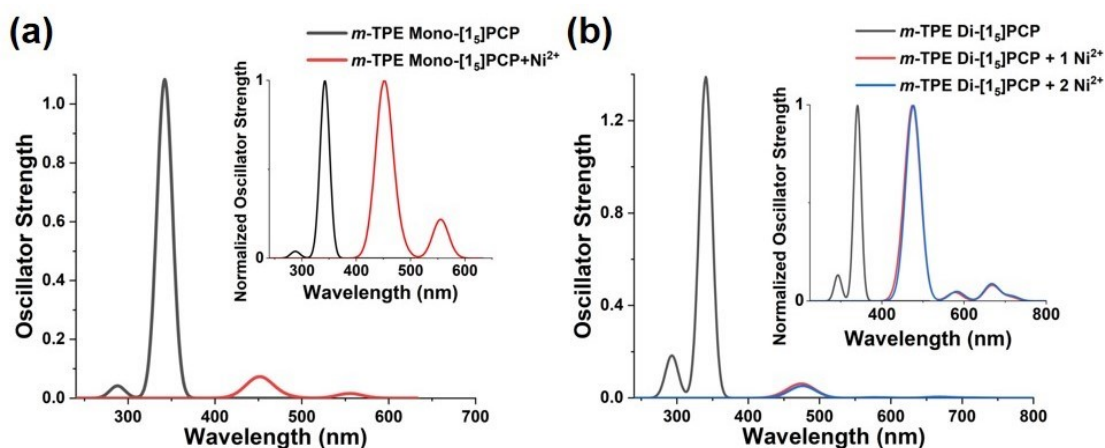

Fig. S39. (a) Electronic transition in the **_m_-TPE Mono-[1₅]PCP** with the addition of Ni ions; Inset showing normalized spectrum of the **_m_-TPE Mono-[1₅]PCP** with and without the addition of Ni ions, (b) Electronic transition in the **_m_-TPE Di-[1₅]PCP** with the addition of Ni ions; Inset showing normalized spectra of the **_m_-TPE Di-[1₅]PCP** with addition of single and double Ni ions.

8. UV-vis spectra
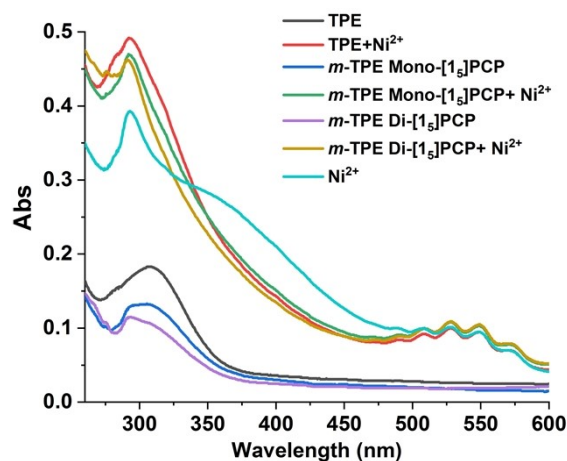
Fig. S40. UV-vis spectra of **TPE**, **_m_-TPE Mono-[1₅]PCP** and **_m_-TPE Di-[1₅]PCP** in 95/5 THF/H₂O mixture (2×10^{-5} M), and their corresponding spectra after adding 5 equiv. Ni^{2+}.

9. MS spectrum for the complex of *m*-TPE Mono-[1₅]PCP with Ni²⁺
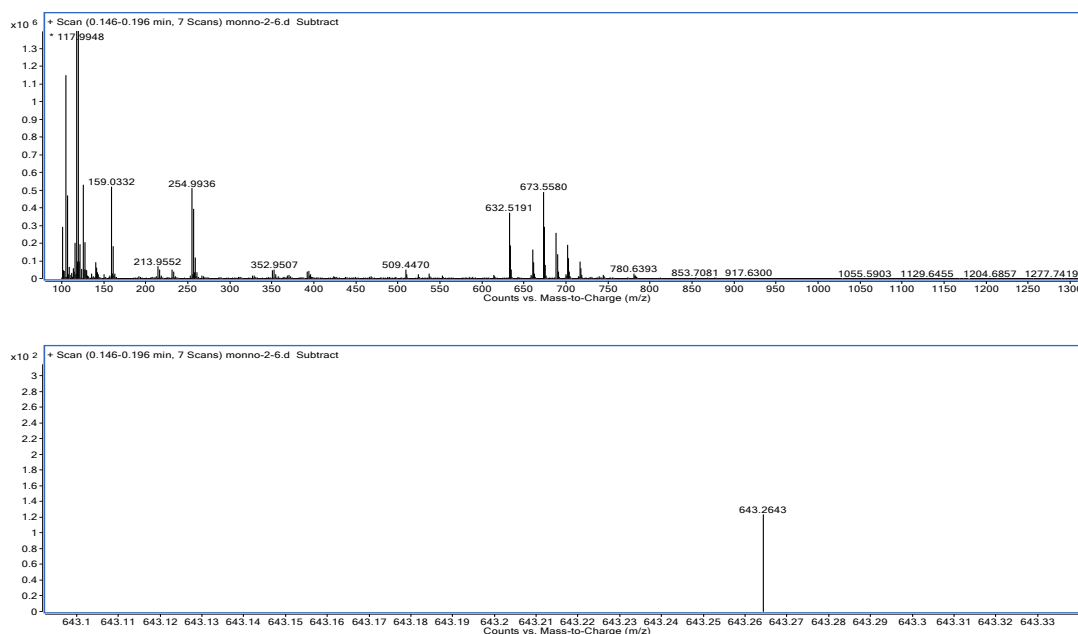
Fig. S41. MS spectrum for ***m*-TPE Mono-[1₅]PCP** with Ni²⁺ (Calculated [2M+Ni]²⁺/2: $C_{96}H_{76}Ni^{2+}/2 = 643.2645$, Found: 643.2643).

10. References

[S1] P. Liu, Q. Li, H. Zeng, B. Shi, J. Liu and F. Huang, *Org. Chem. Front.*, **2019**, 6, 309-312.

[S2] E. Meichsner, I. Nierengarten, M. Holler, M. Chessé and J.-F. Nierengarten, *Helv. Chim. Acta*, **2018**, 101.1800059.

[S3] M. Frisch, G. Trucks, H. Schlegel, G. Scuseria, M. Robb, J. Cheeseman, G. Scalmani, V. Barone, B. Mennucci, G. Petersson, H. Nakatsuji, M. Caricato, X. Li, H. Hratchian, A. Izmaylov, J. Bloino, G. Zheng, J. Sonnenberg, M. Hada, M. Ehara, K. Toyota, R. Fukuda, J. Hasegawa, M. Ishida, T. Nakajima, Y. Honda, O. Kitao, H. Nakai, T. Vreven, J. Montgomery, J. Peralta, F. Ogliaro, M. Bearpark, J. Heyd, E. Brothers, K. Kudin, V. Staroverov, R. Kobayashi, J. Normand, K. Raghavachari, A. Rendell, J. Burant, S. Iyengar, J. Tomasi, M. Cossi, N. Rega, J. Millam, M. Klene, J. Knox, J. Cross, V. Bakken, C. Adamo, J. Jaramillo, R. Gomperts, R. Stratmann, O. Yazyev, A. Austin, R. Cammi, C. Pomelli, J. Ochterski, R. Martin, K. Morokuma, V. Zakrzewski, G. Voth, P. Salvador, J. Dannenberg, S. Dapprich, A. Daniels, Farkas, J. Foresman, J. Ortiz, J. Cioslowski and D. Fox, *Gaussian 09 Revis. B01 Gaussian Inc Wallingford CT* 2009.

[S4] C. Lee, W. Yang and R. G. Parr, *Phy. Rev. B*, **1988**, 37, 785-789.

[S5] B. Miehlich, A. Savin, H. Stoll and H. Preuss, *Chem. Phys. Lett.*, **1989**, 157, 200-206.

[S6] P. C. Hariharan and J. A. Pople, *Theor. Chim. Acta,* **1973**, 28, 213-222.

[S7] W. J. Hehre, R. Ditchfield and J. A. Pople, *J. Chem. Phys.*, **1972**, 56, 2257-2261.